Formation of Aromatic Siloxane Self-Assembled Monolayers

Susan L. Brandow, Mu-San Chen, Charles S. Dulcey, and Walter J. Dressick*

Naval Research Laboratory, Center for Bio/Molecular Science & Engineering, Code 6900, 4555 Overlook Avenue, S.W., Washington, District of Columbia 20375

Received October 24, 2007. In Final Form: December 28, 2007

We describe reproducible protocols for the chemisorption of self-assembled monolayers (SAMs), useful as imaging layers for nanolithography applications, from *p*-chloromethylphenyltrichlorosilane (CMPS) and 1-(dimethylchlorosilyl)-2-(*p*,*m*-chloromethylphenyl)ethane on native oxide Si wafers. Film chemisorption was monitored and characterized using water contact angle, X-ray photoelectron spectroscopy, and ellipsometry measurements. Atomic force microscopy was used to monitor the onset of multilayer deposition for CMPS films, ultimately allowing film macroscopic properties to be correlated with their surface coverage and nanoscale morphologies. Although our results indicate the deposition of moderate coverage, disordered SAMs under our conditions, their quality is sufficient for the fabrication of sub-100-nm-resolution metal features. The significance of our observations on the design of future imaging layers capable of molecular scale resolution in nanolithography applications is briefly discussed.

Introduction

Organotrichlorosilanes are a group of self-assembling materials that can be chemisorbed onto a wide variety of technologically important substrates to modify surface wettability, adhesion, and reactivity.[1] Numerous chemical functional groups are compatible with organotrichlorosilanes and can therefore be attached to a surface as robust films, facilitating applications in fields ranging from chromatography and molecular biology to microelectronics.[2−6] Among these, films containing benzyl halide and pseudohalide functional groups are of particular interest due to their unique reactivities. For example, benzyl halide groups readily participate in nucleophilic displacement reactions,[7,8] making them ideal platforms for immobilization of materials for applications such peptide synthesis (e.g., Merrifield resin)[9] and fabrication of supramolecular architectures exhibiting useful optical properties.[10]

We[11−19] and others[20−25] have been exploring films containing the benzyl chromophore as top-surface imaging layers for high-resolution lithography applications. Specifically, our work in this area exploits the extreme sensitivity of the benzyl carbon−heteroatom bond to cleavage by either photon or electron exposure. For example, deep UV exposure (i.e., ∼248−193 nm)[12−14] of chloromethylphenylsiloxane self-assembled monolayers (SAMs) or polychloromethylstyrene thin films under ambient conditions leads to rapid evolution of HCl and oxidation of the benzyl chromophore to aldehyde and carboxylic acid at doses as low as ∼50 mJ·cm^{-2} (193 nm).[14] Similar dissociation of the C−Cl bond has been noted for films exposed to proximity X-rays[15] or low-energy electrons,[17−19] providing a mechanism for efficient surface patterning of chemical functional groups.

Use of organosiloxane SAMs as imaging layers raises the possibility of image formation where pixels are on the scale of one or several molecules. For example, we have previously demonstrated the formation of features as small as ∼8 nm in the latent image of aromatic *m*,*p*-(aminoethylaminomethyl)phenethylsiloxane (i.e., PEDA) SAMs exposed using the low-energy electrons from a scanning tunneling microscope tip.[17] At these resolutions, it becomes important to have an understanding of surface coverage and intermolecular order in the SAM. The possibility of bulk polymerization, both in solution and at the surface during SAM chemisorption, is also of concern because the increased electrical resistance of multilayered films greatly limits the achievable feature resolution in nanolithography.[26] Consequently, understanding the factors that control SAM formation and developing reproducible means to fabricate and

* Corresponding author. E-mail: wjd@cbmse.nrl.navy.mil.

(1) Onclin, S.; Ravoo, B. J.; Reinhoudt, D. N. *Angew. Chem., Int. Ed.* **2005**, *44*, 6282−6304.
(2) Gun'ko, V. M.; Zarko, V. I.; Leboda, R.; Chibowski, E. *Adv. Colloid Interface Sci.* **2001**, *91*, 1−112.
(3) Bent, S. F. *Surf. Sci.* **2002**, *500*, 879−903.
(4) Sugimura, H. *Int. J. Nanotechnol.* **2005**, *2*, 314−347.
(5) del Campo, A.; Bruce, I. J. *Top. Curr. Chem.* **2005**, *260*, 77−111.
(6) Calvert, J. M.; Dressick, W. J.; Dulcey, C. S.; Chen, M-S.; Georger, J. H.; Stenger, D. A.; Koloski, T. S.; Calabrese, G. S. *A.C.S. Symp. Ser.* **1994**, *537*, 210−219.
(7) Koloski, T. S.; Dulcey, C. S.; Haralson, Q. J.; Calvert, J. M. *Langmuir* **1994**, *10*, 3122−3133.
(8) Brandow, S. L.; Schull, T. L.; Martin, B. D.; Guerin, D. C.; Dressick, W. J. *Chem. Eur. J.* **2002**, *8*, 5363−5367.
(9) Kimmerlin, T.; Seebach, D. *J. Pept. Res.* **2005**, *65*, 229−260.
(10) Facchetti, A.; van der Boom, M. E.; Abbotto, A.; Beverina, L.; Marks, T. J.; Pagani, G. A.; *Langmuir* **2001**, *17*, 5939−5942.
(11) Chen, M-S.; Dulcey, C. S.; Chrisey, L. A.; Dressick, W. J. *Adv. Funct. Mater.* **2006**, *16*, 774−783.
(12) Sun, S. Q.; Montague, M.; Critchley, K.; Chen, M-S.; Dressick, W. J.; Evans, S. D.; Leggett, G. J. *Nano Lett.* **2006**, *6*, 29−33.
(13) Brandow, S. L.; Chen, M-S.; Fertig, S. J.; Chrisey, L. A.; Dulcey, C. S.; Dressick, W. J. *Chem. Eur. J.* **2001**, *7*, 4495−4499.
(14) Brandow, S. L.; Chen, M-S.; Aggarwal, R.; Dulcey, C. S.; Calvert, J. M.; Dressick, W. J. *Langmuir* **1999**, *15*, 5429−5432.
(15) Dressick, W. J.; Dulcey, C. S.; Brandow, S. L.; Witschi, H.; Neeley, P. F. *J. Vac. Sci. Technol. A* **1999**, *17*, 1432−1440.
(16) Dressick, W. J.; Dulcey, C. S.; Chen, M-S.; Calvert, J. M. *Thin Solid Films* **1996**, *285*, 568−572.
(17) Marrian, C. R. K.; Perkins, F. K.; Brandow, S. L.; Koloski, T. S.; Dobisz, E. A.; Calvert, J. M. *Appl. Phys. Lett.* **1994**, *64*, 390−392.
(18) Calvert, J. M.; Koloski, T. S.; Dressick, W. J.; Dulcey, C. S.; Peckerar, M. C.; Cerrina, F.; Taylor, J. W.; Suh, D. W.; Wood, O. R.; MacDowell, A. A.; D'Souza, R. *Opt. Eng.* **1993**, *32*, 2437−2445.
(19) Dressick, W. J.; Calvert, J. M. *Jpn. J. Appl. Phys. Part 1* **1993**, *32(12B)*, 5829−5839.
(20) Weinberger, M. R.; Rentenberger, S.; Kern, W. *Monat. Chem.* **2007**, *138*, 309−314.
(21) Lex, A.; Trimmel, G.; Kern, W.; Stelzer, F. *J. Mol. Catal. A-Chem.* **2006**, *254*, 174−179.
(22) Sugimura, H.; Hong, L.; Lee, K-H. *Jpn. J. Appl. Phys. Part 1* **2005**, *44(7A)*, 5185−5187.
(23) Weinberger, M. R.; Langer, G.; Pogantsch, A.; Haase, A.; Zojer, E.; Kern, W. *Adv. Mater.* **2004**, *16*, 130−133.
(24) Saito, N.; Hayashi, K.; Sugimura, H.; Takai, O. *J. Mater. Chem.* **2002**, *12*, 2684−2687.
(25) Higashi, J.; Nakayama, Y.; Marchant, R. E.; Matsuda, T. *Langmuir* **1999**, *15*, 2080−2088.
(26) Madou, M. J. *Fundamentals of Microfabrication: The Science of Miniaturization*, 2nd ed.; CRC Press: Boca Raton, FL, 2002; Chapter 1, pp 55−63, and references therein.

10.1021/la703326m
Published on Web 02/27/2008

Scheme 1. CMPS and ECMPS Organosilane Structures and Dimensions

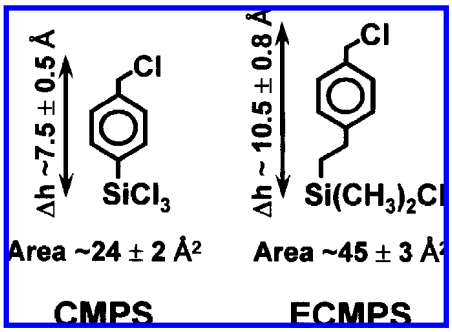

characterize SAMs are critically important for use of these films as nanolithography imaging layers.

In this paper, we address the problems of reproducibly fabricating aromatic siloxane SAM imaging layers using organotrichlorosilanes bearing chloromethylphenyl (CMP) chromophores, such as the trichlorosilane *p*-chloromethylphenyltrichlorosilane (CMPS) and the monochlorosilane 1-(dimethylchlorosilyl)-2-(*m*,*p*-chloromethylphenyl)ethane (ECMPS) (Scheme 1), as model systems. We describe an AFM method for monitoring the progress of chemisorption toward monolayer formation and the deposition of siloxane oligomers leading to the onset of multilayer formation. Correlation of the growing film's macroscale properties, such as sessile water drop contact angle (θ_w), with its nanoscale morphology provides a convenient means for the use of macroscopic properties to determine the completion point for monolayer deposition. Through variations of substrate treatment conditions such as organotrichlorosilane concentration and deposition time, among others, we are able to identify deposition conditions and protocols leading to reproducible deposition of SAMs for these materials.

Experimental Section

Substrates and Materials. All chemicals were ACS reagent grade and were used as received except where noted. N_2 gas was liquid N_2 boil-off and water was deionized (18 MΩ cm resistivity). Anhydrous toluene was Aldrich SureSeal, and acetonitrile was Burdick and Jackson HPLC grade. CMPS (142−144 °C; 15 mmHg) and ECMPS (134−135 °C, 20 mmHg) were from United Chemical Technologies Inc. or Gelest Inc. and were purified by vacuum distillation immediately prior to use. Fused silica slides (25 mm × 25 mm × 1 mm; Dell Optics, Fairview, NJ) and native oxide Si wafers (p-type, ⟨100⟩, 4−7 Ω·cm resistivity, 4 in. diameter; Wafernet Inc., San Jose, CA) were cleaned immediately prior to use for SAM chemisorption according to the literature procedure.[15] The NIPOSIT 468B commercial electroless Ni bath from Rohm & Haas (Shipley Division) was prepared according to the manufacturer's instructions and then diluted to 10% strength with water at pH 7 for use at room temperature. The Pd electroless catalyst dispersion was prepared according to the method described elsewhere.[27]

Film Formation. Chemisorption of CMPS and ECMPS SAMs to fused silica slides or Si wafers was carried out at 22 ± 2 °C under N_2 atmosphere in a glove box (<1 ppm O_2, 2−5 ppm H_2O; Model LM-100, Innovative Technology Inc.). All glassware and UV cuvettes were vapor primed with hexamethyldisilazane using the literature procedure[15] to minimize depletion of solution [CMPS] and [ECMPS] via chemisorption to the sample treatment glassware. Cleaned fused silica or Si wafer substrates were removed from storage in gently boiling water, dried with a filtered stream of N_2 gas, and loaded onto a cassette, which was immediately transferred into a jar containing sufficient toluene to cover the substrates. The jar was loosely sealed and transferred into the glove box, where the cassette and substrates were placed in a beaker containing a toluene solution of CMPS or ECMPS to initiate chemisorption. Solution concentrations of CMPS or ECMPS and treatment times depended on the experiment, as described in the text, and ranged from 0.01 to 5% (vol) and 1 min to 26 h, respectively. The treated substrates were removed from the organosilane solution and subjected to toluene rinsing protocols described in the text, stored under toluene during removal from the glove box, immediately removed from the toluene, and dried in the filtered N_2 gas stream before being baked at 120 °C either in an oven for 4−6 min or on a DATAPLATE Model 721P hotplate for 3−4 min to complete the chemisorption process.

Film Characterization. Extinction coefficients at the 195 nm absorbance maximum of the benzyl chloride chromophore [$\epsilon = (5.50 \pm 0.10) \times 10^4\,L{\cdot}mol^{-1}{\cdot}cm^{-1} \equiv (5.50 \pm 0.10) \times 10^7\,cm^2{\cdot}mol^{-1}$] were calculated from Beer's law using $b = 1.00$ cm path length quartz cuvettes and CH_3CN solutions containing known concentrations of CMPS or ECMPS. Ellipsometric measurements of the SAMs on Si wafers were made using an instrument and protocols described previously,[28] with film thicknesses (average ± 3σ of 9 measurements per substrate) calculated using refractive indices for CMPS ($\eta_D = 1.5395$) and ECMPS ($\eta_D = 1.5223$) supplied by the manufacturer. Molecular dimensions and cross-sectional areas were estimated for energy-minimized structures of CMPS and ECMPS using ChemDraw/ChemBats3D (CambridgeSoft, Cambridge, MA) modeling programs. Sessile water drop contact angles (θ_w) were average values for five measurements per substrate made using 10 μL drops at 22 ± 2 °C and an NRL Zisman-type contact angle goniometer. UV−visible absorbance and XPS measurements were made using instruments and procedures described elsewhere.[29] CMP chromophores in films chemisorbed to our Si wafer substrates exhibited negligible Cl loss (i.e., <2%) during XPS measurements. High-resolution AFM images of SAMs chemisorbed on low roughness, polished Si wafers (rms < 0.1 nm over a 1 μm × 1 μm area) were acquired at 22 ± 2 °C in tapping mode using a Nanoscope III AFM equipped with microfabricated silicon nitride cantilevers (Digital Instruments, Santa Barbara, CA). Samples were immersed in water and imaged using the fluid cell attachment to minimize contamination and scanning force required (i.e., 1−3 nN). A 15 nm × 15 nm image was acquired and then cropped to a 10 nm × 10 nm size. Data processing included corrections for image distortion due to the finite tip size and a planefit and 3 × 3 median filter. Cross-sections were taken across the image to measure the peak-to-peak height.

The performance of the CMPS SAM as an imaging layer for fabrication of patterned electroless Ni films was used to assess the quality and utility of the CMPS SAM we prepared here. Briefly,[29] native oxide Si wafers bearing chemisorbed CMPS SAMs were immersed for ~3 h at room temperature in ~0.1 M pyridine (aq) solution to physisorb pyridine ligand into nanocavity defect sites present in the SAM. The treated substrates were dried in a stream of filtered N_2 gas and transferred into a JEOL JBX 5DII e-beam nanowriter, where displacement of the physisorbed pyridine during electron exposure (500 μC·cm^{-2}; 50 keV) created latent image line features having widths ranging from 2 μm to ~30 nm in the CMPS SAM. Subsequent treatment of the samples at room temperature with Pd catalyst for ~2 h, followed by rinsing in water and immersion in the electroless Ni bath for ~6 min, led to selective Ni deposition on the unexposed regions of the SAM. The patterned Ni films were then rinsed in water, dried in a filtered N_2 gas stream, and placed in a Plasmatherm 500 reactive ion etcher, where they were plasma etched (16 sscm:12 sscm SF_6:CHF_3, 45 W, 18 mTorr, ~35 min) to a depth of ~0.25 μm into the Si substrate to improve image contrast and assess the durability of the Ni films. The quality of the etched Ni films and patterning process selectivity were evaluated using a Leica field emitter scanning electron microscope (SEM).

(27) Dressick, W. J.; Chen, M-S.; Brandow, S. L.; Rhee, K. W.; Shirey, L. M.; Perkins, F. K. *Appl. Phys. Lett.* **2001**, *78*, 676−678.

(28) Dressick, W. J.; Dulcey, C. S.; Georger, J. H.; Calabrese, G. S.; Calvert, J. M. *J. Electrochem. Soc.* **1994**, *141*, 210−220.

(29) Chen, M-S.; Brandow, S. L.; Schull, T. L.; Chrisey, D. B.; Dressick, W. J. *Adv. Funct. Mater.* **2005**, *15*, 1364−1375.

Results and Discussion

This study was initiated as a result of our interest in utilizing aromatic organosiloxane SAMs as imaging layers for high-resolution lithography.[11,12,14−19,29−33] Exposure to patterned radiation removes or transforms SAM functional groups, generating patterns of chemical reactivity on the surface that can be used to selectively bind materials of interest.[28−34] SAM films are clearly preferable for such applications in order to minimize the radiation dose required to alter film chemistry and maximize feature resolution.[17,26] In the course of our work with aromatic siloxane SAMs, however, we noticed a dependence of film quality and thickness on the chemisorption conditions (e.g., humidity, solvent, organosilane solution concentration, deposition time). In the following discussion, we first describe our general observations concerning the effect of these parameters on SAM formation using CMP siloxanes as model systems. From this, we establish a protocol for reproducibly depositing SAM films of CMP siloxanes. Finally, we describe the analytical techniques used to characterize the SAMs and correlate macroscopic film properties with nanoscale film morphology.

It is well-known that chemisorption of *n*-alkyltrichlorosilanes from solution onto oxide surfaces is influenced by numerous factors, including temperature,[35] humidity,[36,37] organotrichlorosilane solution concentration,[37,38] solvent,[39−42] substrate (i.e., surface hydroxyl type[43,44] and density[43−45]), and water levels in the solvent[40,46] and at the substrate[45,47] surface. For *n*-alkyltrichlorosilanes, favorable van der Waals interactions between methylene groups in the adjacent alkyl chains also influence order and packing of the resultant SAM.[39,41,42] In general, reproducible formation of densely packed alkylsiloxane SAMs is favored using dilute solutions of organotrichlorosilanes in dry solvents with substrates bearing sufficient reactive surface silanol groups (i.e., 4−5 Si−OH/ nm^2) wetted by several monolayers of adsorbed H_2O. Such conditions minimize solution-phase organotrichlorosilane hydrolysis and condensation, leading to siloxane-bridged oligomers, which promote multilayer growth when subsequently chemisorbed to the surface and maximize direct hydrolysis and siloxane formation at the substrate surface Si−OH sites, as required for deposition of homogeneous SAMs.

In our initial experiments, we confirmed chemisorption behavior for CMPS similar to that previously observed for alkyltrichlorosilanes. For example, CMPS solutions prepared using toluene pre-equilibrated several hours to days in air (relative humidity 55 ± 5%), especially those containing ≥1% vol CMPS, increasingly led to deposition of patchy, white, macroscopic CMP siloxane multilayer films. Poor-quality films were similarly observed on substrates rigorously dried by baking (120−150 °C; 15−120 min) prior to CMPS deposition, confirming the importance of substrate surface hydration in the chemisorption process. Therefore, we conducted subsequent experiments in a drybox (2−5 ppm H_2O) using cleaned Si wafer or fused silica substrates dried in a stream of filtered N_2 gas, anhydrous toluene (<0.005% H_2O) containing 0.01−1.0% vol CMPS for film deposition, and anhydrous toluene for post-CMPS treatment substrate rinses to control moisture levels.

Previous alkyltrichlorosilane work supports a chemisorption mechanism involving initial hydrolysis of Si−Cl bonds to form alkyltrisilanols at the hydrated substrate, followed by self-assembly of organized, transient, physisorbed Langmuir-type alkyltrisilanol multilayers at the surface stabilized by silanol−water hydrogen bonding and van der Waals interactions among the alkyl components.[35,44−47] Collapse of the hydrogen-bonded silanol network to form covalent siloxane bonds during a baking step after removal of the substrate from the treatment solution then completes the chemisorption reaction. Consequently, adequate rinsing of the substrate to remove loosely physisorbed species from those comprising the layer adjacent to the surface prior to heat curing is critically important for SAM formation. For our CMPS films, we observed that as much as 50% of the deposited CMPS can be removed prior to substrate baking through vigorous rinsing with toluene, consistent with this mechanism. We eventually determined that a triple rinse of CMPS-treated substrates via sequential >30 s immersions in fresh portions of toluene was sufficient to remove this physisorbed material, leading to reproducible CMP siloxane film formation, as measured by θ_w, AFM, XPS, UV absorbance (195 nm), or ellipsometry (vide infra).

On the basis of these initial observations concerning CMPS behavior, we adapted the general alkyltrichlorosilane chemisorption model to describe aromatic trichlorosilane chemisorption, as shown in Figure 1. In this model, the initial substrate surface bearing hydrated isolated, vicinal (both colored green), and geminal (red) silanol groups,[48−50] designated as surface A, is treated with a toluene solution of the CMPS trichlorosilane in step 1. Hydrolysis of CMPS to form the corresponding trisilanol species occurs at the hydrated substrate surface followed by chemisorption of the CMP aromatic functional group (orange) to the surface, as shown in surface B. Oligomeric siloxane species, formed via partial trichlorosilane hydrolysis by trace water and silanol condensation in the toluene solution phase, can also chemisorb CMP organofunctional groups (yellow) onto the surface. Surface adsorption of additional CMPS from the solution in step 2, ultimately leading to siloxane bond formation with the Si−OH sites on the substrate surface and free silanol sites of the initially chemisorbed species, completes the CMP monolayer (white) formation in surface C.

(30) Dulcey, C. S.; Georger, J. H.; Chen, M-S.; McElvany, S. W.; O'Ferrall, C. E.; Benezra, V. I.; Calvert, J. M. *Langmuir* **1996**, *12*, 1638−1650.
(31) Friedli, A. C.; Roberts, R. D.; Dulcey, C. S.; Hsu, A. R.; McElvany, S. W.; Calvert, J. M. *Langmuir* **2004**, *20*, 4295−4298.
(32) Dressick, W. J.; Nealey, P. F.; Brandow, S. L. *Proc. SPIE* **2001**, *4343*, 294−305.
(33) Koumoto, K.; Seo, S.; Sugiyama, T.; Seo, W. S.; Dressick, W. J. *Chem. Mater.* **1999**, *11*, 2305−2309.
(34) Ma, D. I.; Shirey, L.; McCarthy, D.; Thompson, A.; Qadri, S. B.; Dressick, W. J.; Chen, M-S.; Calvert, J. M.; Kapur, R.; Brandow, S. L. *Chem. Mater.* **2002**, *14*, 4586−4594.
(35) Brzoska, J. B.; Azouz, I. B.; Rondelez, F. *Langmuir* **1994**, *10*, 4367−4373.
(36) Harada, Y.; Girolami, G. S.; Nuzzo, R. G. *Langmuir* **2004**, *20*, 10878−10888.
(37) Rozlosnik, N.; Gerstenberg, M. C.; Larsen, M. B. *Langmuir* **2003**, *19*, 182−188.
(38) Bunker, B. C.; Carpick, R. W.; Assink, R. A.; Thomas, M. L.; Hankins, M. G.; Voigt, J. A.; Sipola, D.; de Boer, M. P.; Gulley, G. L. *Langmuir* **2000**, *16*, 7742−7751.
(39) Duchet, J.; Chabert, B.; Chapel, J. P.; Gérard, J. F.; Chovelon, J. M.; Jaffrezic-Renault, N. *Langmuir* **1997**, *13*, 2271−2278.
(40) Rühe, J.; Novotny, V. J.; Kanazawa, K. K.; Clarke, T.; Street, G. B. *Langmuir* **1993**, *9*, 2383−2388.
(41) Kallury, K. M. R.; Thompson, M.; Tripp, C. P.; Hair, M. L. *Langmuir* **1992**, *8*, 947−954.
(42) Gun, J.; Sagiv, J. *J. Colloid Interface Sci.* **1986**, *112*, 457−472.
(43) van Velzen, P. N. T.; Ponjeé, J. J.; Benninghoven, A. *Appl. Surf. Sci.* **1989**, *37*, 147−159.
(44) Wang, R.; Wunder, S. L. *Langmuir* **2000**, *16*, 5008−5016.
(45) Wang, R.; Guo, J.; Baran, G.; Wunder, S. L. *Langmuir* **2000**, *16*, 568−576.
(46) McGovern, M. E.; Kallury, K. M. R.; Thompson, M. *Langmuir* **1994**, *10*, 3607−3614.
(47) Tripp, C. P.; Hair, M. L. *Langmuir* **1995**, *11*, 1215−1219.
(48) Scholten, A. B.; de Haan, J. W.; Claessens, H. A.; van de Ven, L. J. M.; Cramers, C. A. *Langmuir* **1996**, *12*, 4741−4747.
(49) Linton, R. W.; Miller, M. L.; Maciel, G. E.; Hawkins, B. L. *Surf. Interface Anal.* **1985**, *7*, 196−203.
(50) Sindorf, D. W.; Maciel, G. E. *J. Phys. Chem.* **1982**, *86*, 5208−5219.

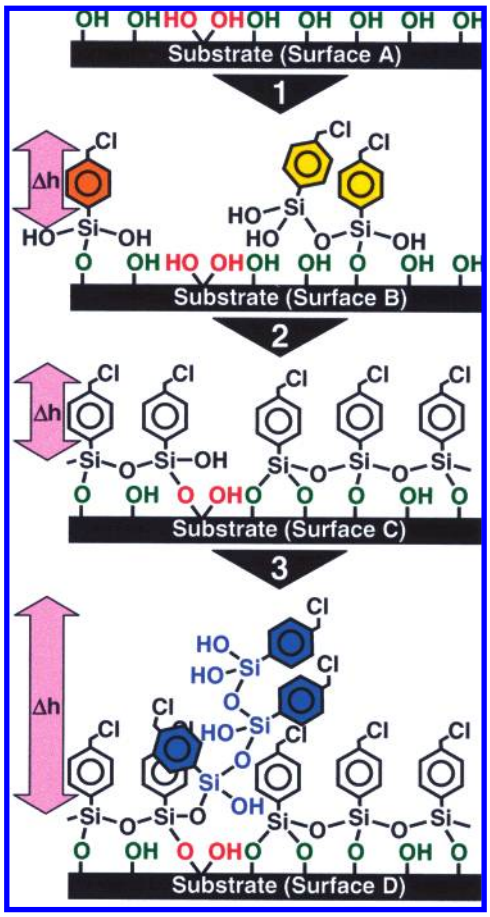

Figure 1. CMPS surface chemisorption model. Different types of surface Si−OH sites on a clean native oxide Si wafer (surface A) provide reactive sites for chemisorption (surface B) of monomeric and oligomeric CMPS solution species following their hydrolysis by adsorbed water (not shown for clarity) at the wafer surface. Organization of the growing CMPS film is governed by hydrogen-bond-network formation among the CMPS trisilanol and surface Si−OH groups and intercalation of toluene solvent among the CMP groups (both not shown for clarity) of the nascent film[29] prior to Si−O−Si siloxane bond formation. The resulting chemisorbed CMPS SAM (surface C) contains defects templated by the types and distribution of the surface Si−OH groups and the toluene solvent during film deposition. Solution accessible surface Si−OH sites at some of these defects, such as the geminal Si−OH site (i.e., designated by the red OH) shown here, provide nucleation sites for the continued chemisorption of CMPS leading to multilayer film formation (surface D). Consult the text for further details.

The quality (i.e., defect density) of the monolayer depicted by surface C will be influenced by at least three factors. First, lateral CMP film growth promoted by condensation of incoming CMPS trisilanol species with reactive silanols present on the initially chemisorbed (orange/yellow) species on surface B leads to domain boundary defects as growing CMP islands meet during the chemisorption process.[51,52] Second, point defects can also occur due to variations in the local density and type of Si−OH groups present on the substrate surface. For example, although one hydroxyl group from a geminal Si−OH readily forms a siloxane bond, reaction of the second hydroxyl group will be sterically hindered,[43,48−50] creating a potential point defect in the monolayer, as shown in surface C. Finally, we have previously shown that intercalation of aromatic solvents via reversible, noncovalent (e.g., $\pi-\pi$ or van der Waals) interactions with previously

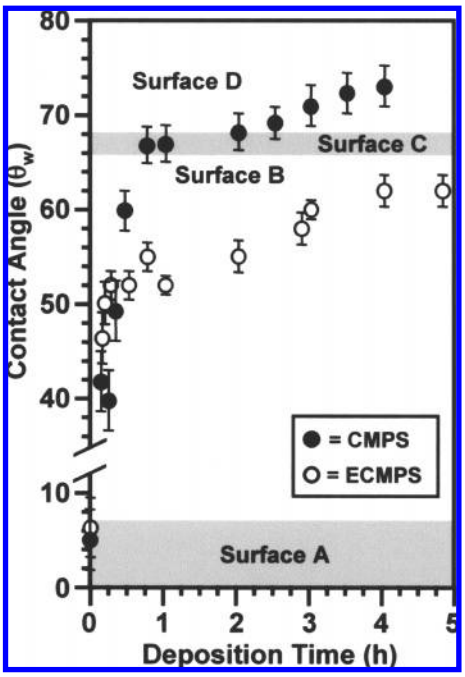

Figure 2. Chemisorption growth curves for CMPS and ECMPS films. Film growth as a function of solution treatment time is monitored by sessile water drop contact angle (θ_w) on treated native oxide Si wafers. The optimized treatment protocol for reproducible film deposition is (1) removal of a clean[15] native oxide Si wafer from storage in water, (2) drying of the wafer surface in a N_2 gas stream, (3) immersion of the wafer in toluene and transfer under toluene into a drybox, (4) immersion of the wafer in a toluene solution containing either CMPS (0.01% vol) or ECMPS (1% vol) inside the drybox for the time indicated, (5) sequential 30 s rinses of the treated substrates in three separate portions of fresh toluene, (6) removal of the wafer while submerged in the last toluene rinse from the drybox, (7) drying of the wafer surface in a N_2 gas stream, and (8) baking of the wafer in an oven at 120 °C for ∼4−6 min to complete the chemisorption process. The regions identified as surfaces A−D correspond approximately to designations in the model for CMPS films shown in Figure 1.

chemisorbed aromatic CMP groups during the chemisorption process can influence CMP packing and defect densities in the monolayer film.[27,29,53] Reactive silanol sites remaining within such defects can act as potential nucleation sites for deposition of additional CMP film. Consequently, any hydrolyzed monomeric or oligomeric CMPS species present in the solution phase accessing reactive silanol species at such defect sites can nucleate multilayer growth of CMP (blue) film, as shown in step 3 and surface D.

Using the model of Figure 1 as a guide, it is possible to interpret the results of our chemisorption experiments and determine conditions for formation of CMPS and ECMPS SAMs. For example, Figure 2 describes the optimum protocol developed for reproducible CMP siloxane deposition (±5%) based on our observations and illustrates the deposition of CMPS and ECMPS on Si wafers, as measured by θ_w, as a function of treatment time. Both the trichlorosilane CMPS and monochlorosilane ECMPS initially bind rapidly to the surface, with 0.01% vol CMPS producing a film having $\theta_w \sim 66°$ in ∼1 h and 1% vol ECMPS providing a film with $\theta_w \sim 52°$ after ∼15 min. This behavior is consistent with rapid siloxane condensation of silanol sites on incoming monomeric ECMPS and monomeric or oligomeric CMPS solution species with the large numbers of accessible surface Si−OH sites on surface B of Figure 1.

(51) Bautista, R.; Hartmann, N.; Hasselbrink, E. *Langmuir* **2003**, *19*, 6590−6593.
(52) Liu, Y.; Wolf, L. K.; Messmer, M. C. *Langmuir* **2001**, *17*, 4329−4335.
(53) Dressick, W. J.; Chen, M-S.; Brandow, S. L. *J. Am. Chem. Soc.* **2000**, *122*, 982−983.

The initial rapid deposition stage in Figure 2 is followed by a much slower accumulation of material with increasing treatment times as the substrate surface becomes more fully coated by CMPS or ECMPS. Because there are now fewer surface Si−OH groups available for reaction with incoming CMPS or ECMPS species, as shown for surface C of Figure 1, the chemisorption rate slows and θ_w changes little for the CMPS (i.e., $\theta_w \sim 66-68°$) or ECMPS (i.e., $\theta_w \sim 54-58°$) films. Although these films are essentially "monolayers" according to the simple model of surface C in Figure 1, they have not yet attained their equilibrium (i.e., minimum free energy) configurations. During this time, chemisorption of additional CMPS or ECMPS species onto the surface can occur, but it requires prior reorganization of the network of physisorbed (hydrogen-bonded) aromatic silanol species at the surface and/or displacement of any intercalated toluene solvent to access reactive surface silanol groups. For ECMPS, which is limited by its single reactive Si−Cl site to deposition of a true monolayer film, this chemisorption of additional material slowly occurs with increased treatment time until a limiting value of $\theta_w \sim 64°$ characteristic of the equilibrium SAM is eventually observed. In contrast, although θ_w values for CMPS also continue to slowly increase with treatment time, the ability of the CMPS trisilanol species to form multiple siloxane cross-links as shown for surface D of Figure 1 ultimately leads to the formation of patchy, hazy, white multilayer films on the wafer surface.

Consequently, a means is required to identify the optimal treatment time in Figure 2 for CMPS-based deposition of a complete SAM having minimal multilayer defect sites. We adapted AFM methods,[54−56] which have been used previously to monitor island and monolayer deposition through measurements of surface coverage and film thickness, for this purpose. Si wafers treated with CMPS solution for various times and processed according to the protocol described in Figure 2 were analyzed by AFM as summarized in Figure 3A, which illustrates the dependence of the *maximum* tip displacement (∝film thickness) observed on relative film surface coverage (∝cos θ_w). For short CMPS treatment times (i.e., $\theta_w \rightarrow 0°$ in Figure 2; cos $\theta_w \rightarrow 1$ in Figure 3A), the surface density of substrate silanol sites will be high according to the model of Figure 1 (i.e., surfaces A and B). Chemisorption of the structurally rigid CMPS species to the surface under these conditions will lead to an AFM tip displacement corresponding to the Δh ∼7.5 Å height of the CMP functional group, as shown (i.e., tip displacement ∼7 ± 1 Å) in Figure 3A. Identical behavior occurs as additional CMP groups are chemisorbed until films having $\theta_w \rightarrow 66-68°$ (i.e., cos $\theta_w \rightarrow 0.41-0.38$) are deposited, indicating that CMPS species contacting the surface can apparently be successfully incorporated into the growing film without significant multilayer formation. For longer treatment times (i.e., $\theta_w > 68°$ in Figure 2; cos $\theta_w < 0.38$ in Figure 3A), however, the maximum AFM tip displacement observed in Figure 3A increases rapidly, consistent with increased film thickness due to growth of CMPS multilayers from silanols present at surface defect sites according to the model of surface D in Figure 1.

In contrast, simpler behavior is observed in Figure 3A for surfaces treated by ECMPS, consistent with the inability of this species to form multilayer films. In this case, the maximum tip displacement observed gradually increases as ECMP chemisorbs

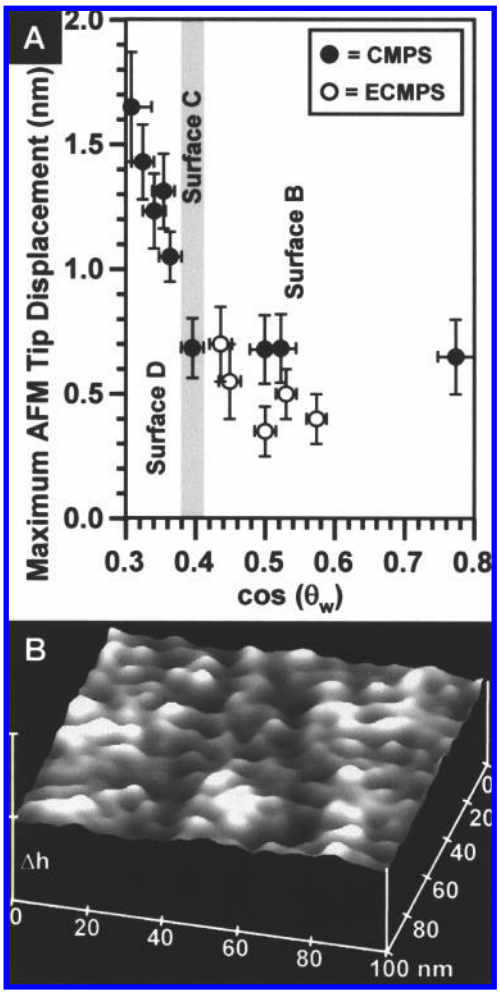

Figure 3. AFM coverage study for CMPS and ECMPS films. (A) *Maximum* AFM tip displacement observed as a function of relative film surface coverage measured by cos θ_w for selected CMPS and ECMPS films from Figure 2 is shown. The regions identified as surfaces A−D correspond approximately to designations in the model for CMPS films shown in Figure 1. (B) AFM scans of a region of the CMPS SAM at a relative surface coverage of cos $\theta_w \sim 0.39$ (i.e., $\theta_w \sim 67°$) in part A corresponding approximately to monolayer coverage depicted by surface C in Figure 1. Vertical scale = 0.7 nm/division. The CMPS film shown corresponds to a ∼75 min treatment time in Figure 2.

to the bare Si wafer ($\theta_w \sim 0°$; cos $\theta_w \sim 1$) until an ECMPS SAM is formed ($\theta_w \sim 64°$; cos $\theta_w \sim 0.44$), after which no further changes occur with increasing solution treatment time. The measured tip displacement for the ECMPS SAM of ∼7.0 ± 1.5 Å is identical to that noted for the CMPS films associated with surfaces B and C of Figure 1, even though the ∼10.5 Å molecular height of ECMPS exceeds that of CMPS (i.e., ∼7.5 Å; Scheme 1). We interpret these results in terms of reorientation of the CMP groups of the ECMPS film in the fluid cell during the AFM measurement to enhance $\pi-\pi$ interactions between adjacent aromatic CMP groups facilitated by (1) the flexible ECMPS ethyl spacer and (2) a lower ECMPS film packing density (vide infra, Figure 4) due to the larger footprint estimated (note Scheme 1) for ECMPS (i.e., ∼45 Å^2 ·molecule^{-1}) compared to CMPS (i.e., ∼24 Å^2·molecule^{-1}). Ellipsometry measurements of the ECMPS SAM thickness in air yield a value of ∼3 ± 1 Å, consistent with a more complete reorientation of the dry film in which adjacent aromatic rings lie more nearly parallel to the substrate surface to maximize $\pi-\pi$ interactions and our interpretation.

(54) Ruths, M.; Alcantar, N. A.; Israelachvili, J. N. *J. Phys. Chem. B* **2003**, *107*, 11149−11157.
(55) Doudevski, I.; Hayes, W. A.; Schwartz, D. K. *Phys. Rev. Lett.* **1998**, *81*, 4927−4930.
(56) Woodward, J. T.; Schwartz, D. K. *J. Am. Chem. Soc.* **1996**, *118*, 7861−7862.

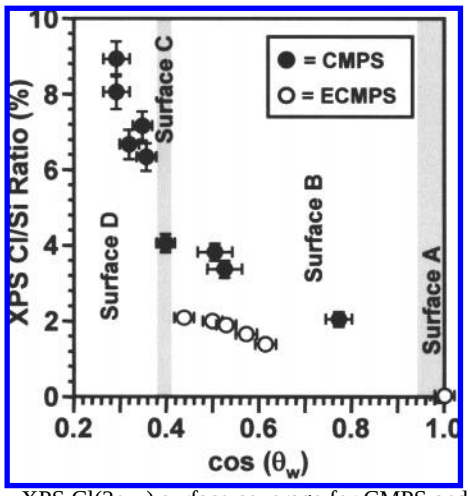

Figure 4. XPS Cl($2p_{3/2}$) surface coverage for CMPS and ECMPS films. The Cl/Si XPS signal intensity is shown as a function of relative surface coverage measured by cos θ_w for selected CMPS and ECMPS films from Figures 2 and 3. In all cases, the XPS Cl($2p_{3/2}$) signal comprises a single component at ~199.9 eV corresponding to the Cl present in the chloromethylphenyl surface functional groups of CMPS and ECMPS. The absence of a signal at ~198 eV ascribed to the chloride ion is consistent with complete hydrolysis of the Si−Cl bonds with removal of the Cl as HCl under our treatment conditions. This is confirmed by Si(2p) XPS results, which comprise a single peak at ~103.1 eV due to the siloxane-cross-linked CMP chromophores, with no peaks at ~101.8−102.5 eV characteristic of Si−Cl species. The regions identified as surfaces A−D correspond approximately to designations in the model for CMPS films shown in Figure 1.

The film growth behaviors described in Figure 3A strongly suggest that formation of the CMPS SAM illustrated by surface C in Figure 1 is essentially complete for films having cos $\theta_w \sim$ 0.41−0.38 (i.e., $\theta_w \sim$ 66−68° in Figure 2). Support for this assignment is shown in the AFM scan of a CMPS film having cos $\theta_w \sim$ 0.39 (i.e., $\theta_w \sim$ 67°) in Figure 3B. For this film, the maximum AFM tip displacement is ~7 ± 1 Å over much of the scanned region, as expected for a CMPS film of monolayer thickness. Thickness measurements via ellipsometry yield values of 8 ± 1 Å, in good agreement with the AFM values, indicating relatively uniform film deposition over the entire Si wafer. In addition, film morphology in Figure 3B clearly shows areas of diminished height, consistent with the presence of defects associated with previously identified film growth mechanisms[27,29,43,48−53] and the model of Figure 1.

Although our results indicate that θ_w and ellipsometry measurements together are sufficient to establish SAM formation and uniformity as described by the model of surface C in Figure 1, additional information concerning the characteristics of the SAM formed requires alternative techniques. For example, knowledge of the molecular packing density of the SAM is critically important for various applications, such as fabrication of array biosensors[57,58] and nanolithography imaging layers,[19,26,59,60] because the surface density of organofunctional groups can influence their reactivity[7,61−65] and limit the feature sizes attainable via SAM patterning.[17,19,66,67] Unfortunately, the cos θ_w values used in Figure 3 provide only a relative measure of surface coverage, which is insufficiently quantitative for these applications.

Therefore, we performed XPS Cl($2p_{3/2}$) measurements of our films, which can be used to quantify film surface coverage (vide infra), and correlated them to cos θ_w values as shown in Figure 4. The behavior of the XPS Cl($2p_{3/2}$) data in Figure 4 is similar, but not identical, to that shown for the AFM data in Figure 3. In both cases, chemisorption of the ECMPS SAM is complete for films having cos $\theta_w \sim$ 0.44 and the CMPS film data exhibit regions of distinctly different behavior as a function of cos θ_w bracketing the SAM breakpoint at cos $\theta_w \sim$ 0.40. However, because the XPS signal is proportional to the *amount* of the CMP film on the surface, it increases monotonically with increasing treatment time (i.e., decreasing cos θ_w) for the CMPS film region 0.40 < cos $\theta_w \leq$ 1.0, corresponding to surfaces A and B of Figure 1. In addition, the CMP group surface aerial density (∝XPS Cl($2p_{3/2}$) signal intensity) is nearly twice that for the CMPS SAM (cos $\theta_w \sim$ 0.40) as for the ECMPS SAM (cos $\theta_w \sim$ 0.44), consistent with the differences in molecular footprints for these species (note Scheme 1). In contrast, because the AFM signal is proportional to the *maximum film thickness*, it remains relatively constant in this region for the more rigid CMPS films but increases somewhat with decreasing cos θ_w for the more flexible ECMPS films (vide supra).

In order to relate the XPS Cl($2p_{3/2}$) surface compositions in Figure 4 to CMP packing densities in our SAMs, we initially attempted to directly measure Cl atom surface density via Rutherford backscattering spectroscopy. Unfortunately, SAM degradation via Cl loss during the experiment yields irreproducible results.[7] Therefore, we have utilized UV−visible absorbance measurements, in conjunction with Hoernschemeyer's equation,[68] to quantify CMP surface coverage for our SAMs. Hoernschemeyer's equation relates θ_w values on two solid surfaces, "F" and "S", as shown in eq 1:

$$(1 + \cos \theta_w{}^F) \cong (\rho_F/\rho_S)(\gamma_F/\gamma_S)^{0.5}[(\sigma_w + \sigma_F)/(\sigma_w + \sigma_S)]^2(1 + \cos \theta_w{}^S) \quad (1)$$

For our systems, we designate the symbols F and S in eq 1 for parameters associated with SAMs deposited on fused silica and native oxide Si wafer substrates, respectively. The subscript "w" in eq 1 refers to parameters associated with the water droplet interacting with the SAM-covered surfaces, the "ρ" are the surface densities (i.e., coverages) of the SAM molecules, the "γ" are the interaction energies of the surface species with the water droplet, and the "σ" are the collision diameters of the surface species and the water droplet molecules.

If ECMPS, which is restricted to monolayer formation due to its single Si−Cl bond, is chemisorbed to *each* of the F and S substrates, eq 1 can be simplified and applied to quantify the CMP group surface coverage in Figure 4. Under these conditions, eq 1 predicts that variations in the ρ, γ, and/or σ parameters for the chemisorbed ECMPS SAMs will lead to different observed

(57) Blattler, T.; Huwiler, C.; Ochsner, M.; Stadler, B.; Solak, H.; Voros, J.; Grandin, H. M. *J. Nanosci. Nanotechnol.* **2006**, *6*, 2237−2264.
(58) Ariga, K.; Nakanishi, T.; Michinobu, T. *J. Nanosci. Nanotechnol.* **2006**, *6*, 2278−2301.
(59) Mendes, P. A.; Preece, J. A. *Curr. Opin. Colloid Interface Sci.* **2004**, *9*, 236−248.
(60) Bittner, A. M. *Surf. Sci. Rep.* **2006**, *61*, 383−428.
(61) Wayment, J. R.; Harris, J. M. *Anal. Chem.* **2006**, *78*, 7841−7849.
(62) Hozumi, A.; Asakura, S.; Fuwa, A.; Shirahata, N.; Kameyama, T. *Langmuir* **2005**, *21*, 8234−8242.
(63) Charles, P. T.; Vora, G. J.; Andreadis, J. D.; Fortney, A. J.; Meador, C. E.; Dulcey, C. S.; Stenger, D. A. *Langmuir* **2003**, *19*, 1586−1591.
(64) Nivens, D. A.; Conrad, D. W. *Langmuir* **2002**, *18*, 499−504.
(65) Brandow, S. L.; Dressick, W. J.; Chow, G-M.; Marrian, C. R. K.; Calvert, J. M. *J. Electrochem. Soc.* **1995**, *142*, 2233−2243.
(66) Ressier, L.; Martin, C.; Viallet, B.; Grisolia, J.; Peyrade, J-P. *J. Vac. Sci. Technol. B* **2007**, *25*, 17−20.
(67) Brandow, S. L.; Chen, M-S.; Wang, T.; Dulcey, C. S.; Calvert, J. M.; Bohland, J. F.; Calabrese, G. S.; Dressick, W. J. *J. Electrochem. Soc.* **1997**, *144*, 3425−3434.
(68) Hoernschemeyer, D. *J. Phys. Chem.* **1966**, *70*, 2628−2633.

ECMPS SAM θ_w values on each substrate. For example, although siloxane (Si−O−Si) and silanol (Si−OH) species populate the surfaces of both fused silica (i.e., SiO_2) and Si native oxide (i.e., SiO_x, $x < 2$), differences in their internal silicon oxide structures[69−71] will affect the total Si−OH coverage and distributions of the various isolated, vicinal, and geminal Si−OH groups on the surface of each material.[43,48−50,72−74] For ECMPS, chemisorption can *only* occur through reaction of its single Si−Cl bond *directly* with a surface Si−OH species. Consequently, the surface distribution of the various vicinal, isolated, and geminal Si−OH species and differences in their reactivity toward the ECMPS Si−Cl bond,[48−50] together with the degree of solvation[29,32] and geometric constraints of the ECMPS molecule itself,[40,48−50] will influence ρ for the chemisorbed films.

In principle, θ_w will also be influenced by molecular interactions of water with all of the various siloxane, Si−OH, and chemisorbed ECMPS species present on each surface through the γ and σ parameters. In practice, however, water interactions with chemisorbed ECMPS species are most likely to predominate in establishing the effective values for the γ and σ parameters for several reasons. For example, the ECMP groups will be present on the surface in increasingly larger numbers, even as the surface Si−OH population is depleted during the chemisorption reaction, increasing both the hydrophobicity and structural anisotropy near the remaining unreacted surface Si−OH sites. Although water penetration through the SAM still occurs, the surface Si−OH sites will exhibit decreased degrees of freedom in their interactions with that water due to steric "shielding"[75,76] and reorganization of the local water structure[77−79] by the larger ECMPS organofunctional groups, further limiting their contributions to γ and σ in eq 1. In addition, the larger size of the ECMPS groups, combined with their ability to reorient to establish energetically favorable noncovalent (i.e., van der Waals and/or $\pi-\pi$) interactions between adjacent CMP groups[29,32] within the SAM (vide supra), ideally positions them at the outermost regions of the surface and maximizes their contact with the water droplet.[80] Under such conditions, the approximations $\gamma_F \cong \gamma_S$ and $\sigma_F \cong \sigma_S$ are reasonable[80] and the θ_w are related primarily by the ρ_F/ρ_S ratio, as shown in eq 2:

$$(1 + \cos \theta_w{}^F) \cong (\rho_F/\rho_S)(1 + \cos \theta_w{}^S) \quad (2)$$

Equation 2 can be rewritten as eq 3 to express the surface coverage, ρ_S, of the ECMPS SAM chemisorbed to the native oxide Si wafer in Figure 4, in terms of ρ_F for same SAM on the fused silica slide and the corresponding $\theta_w{}^F$ and $\theta_w{}^S$, all of which can be measured:

$$\rho_S \cong \rho_F{\cdot}(1 + \cos \theta_w{}^S)/(1 + \cos \theta_w{}^F) \quad (3)$$

For example, a value of $(2.09 \pm 0.07) \times 10^{-10}$ mol of CMP·cm^{-2} for ρ_F can be determined for the ECMPS SAM chemisorbed on a fused silica slide according to Beer's law in eq 4:

$$\rho_F = A/2\epsilon \quad (4)$$

In eq 4, A (=0.0230 ± 0.0004) and ϵ [=(5.50 ± 0.10) × 10^7 cm^2·mol of CMP^{-1}] are the absorbance and extinction coefficient, respectively, of the ECMPS SAM benzyl chloride chromophore at its absorbance maximum (i.e., λ = 195 nm), and the factor of "2" accounts for the presence of the SAM on both sides of the fused silica slide.

Using the value of $\theta_w{}^F = 73 \pm 2°$ (i.e., $\cos \theta_w{}^F = 0.28 \pm 0.03$) measured for this ECMPS SAM on the fused silica substrate, together with the corresponding value of $\theta_w{}^S = 64 \pm 2°$ (i.e., $\cos \theta_w{}^F = 0.44 \pm 0.03$) for the ECMPS SAM on the native oxide Si substrate from Figure 4, eqs 3 and 4 provide a value of $\rho_S \cong (2.35 \pm 0.19) \times 10^{-10}$ mol of CMP·cm^{-2} [≡(1.42 ± 0.11) × 10^{14} CMP molecules·cm^{-2}] for the coverage of the ECMPS SAM on the native oxide Si wafer. This value is substantially lower than the theoretical coverage of ∼(3.69 ± 0.25) × 10^{-10} mol of CMP·cm^{-2} [≡(2.22 ± 0.15) × 10^{14} CMP molecules·cm^{-2}] calculated[81] from the ECMPS molecular dimensions shown in Scheme 1, consistent with our previous observations[29,32] regarding diminished CMP surface coverage due to intercalation of aromatic solvent in the nascent SAM during chemisorption. However, the fractional surface coverage of ∼0.64 ± 0.09 [i.e., ∼(2.35 ± 0.19) × 10^{-10} mol of CMP·cm^{-2}/(3.69 ± 0.25) × 10^{-10} mol of CMP·cm^{-2}] by these ECMPS groups on the Si wafer compares well with the analogous fractional surface coverage of ∼0.55 ± 0.05 estimated by UV spectroscopy on fused silica,[29,32] in support of our approach and arguments.

The (2.35 ± 0.19) × 10^{-10} mol of CMP·cm^{-2} coverage calculated from eqs 3 and 4 for the ECMPS SAM corresponds to an XPS Cl/Si ratio of 2% (i.e., at $\cos \theta_w \sim 0.44$) in Figure 4 and effectively quantifies the CMP surface coverage, with a 1% Cl/Si ratio corresponding to a CMP group surface density of ∼(1.18 ± 0.10) × 10^{-10} mol of CMP·cm^{-2} [≡(0.71 ± 0.06) × 10^{14} CMP molecules·cm^{-2}]. Therefore, for the 4% Cl/Si ratio corresponding to CMPS SAM at $\cos \theta_w \sim 0.41$ in Figure 4 (i.e., surface C in Figure 1), we calculate a CMP surface coverage of ∼(4.72 ± 0.38) × 10^{-10} mol of CMP·cm^{-2} [≡(2.84 ± 0.22) × 10^{14} CMP molecules·cm^{-2}]. This is once again less than the expected coverage of ∼(6.92 ± 0.60) × 10^{-10} mol of CMP·cm^{-2} [≡(4.17 ± 0.35) × 10^{14} CMP molecules·cm^{-2}] for a close-packed CMPS SAM based on the molecular footprint shown in Scheme 1, but it is consistent with the creation of aromatic solvent-templated interstices among the CMP groups during SAM chemisorption.[29,32]

The reduced CMP surface coverages observed here, together with the film heterogeneity noted in Figure 2B, will clearly limit the utility of the CMPS and ECMPS SAMs as efficient imaging layers at molecular dimensions. However, film heterogeneity, if it occurs undetected over larger areas of the surface, can also adversely affect the performance of the SAMs as imaging layers during patterning of lower resolution features. For example,

(69) Morita, M.; Ohmi, T. *Jpn. J. Appl. Phys. Part 1* **1994**, *33(1B)*, 370−374.
(70) Kim, M. J.; Carpenter, R. W. *J. Mater. Res.* **1990**, *5*, 347−351.
(71) Phillip, H. R.; Taft, E. A. *J. Appl. Phys.* **1982**, *53*, 5224−5229.
(72) McCafferty, E.; Wightman, J. P. *Surf. Interface Anal.* **1998**, *26*, 549−564.
(73) Yamazaki, H.; Takahashi, M. *Surf. Interface Anal.* **1997**, *25*, 937−941.
(74) Lamb, R. N.; Furlong, D. N. *J. Chem. Soc. Faraday Trans. 1* **1982**, *78*, 61−73.
(75) Morrow, B. A.; McFarlan, A. J. *Langmuir* **1991**, *7*, 1695−1701.
(76) Fóti, G.; Kováts, E. Sz. *Langmuir* **1989**, *5*, 232−239.
(77) Urbic, T.; Vlachy, V.; Dill, K. A. *J. Phys. Chem. B* ***2006***, *110*, 4693−4970.
(78) Vaitheeswaran, S.; Yin, H.; Rasaiah, J. C.; Hummer, G. *Proc. Natl. Acad. Sci. U.S.A.* **2004**, *101*, 17002−17005.
(79) Maibaum, L.; Chandler, D. *J. Phys. Chem. B* **2003**, *107*, 1189−1193.
(80) Johnson, R. E.; Dettre, R. In *Surface Colloid Science;* Matijević, E., Ed.; Wiley-Interscience: New York, 1969; Vol. 2, pp 85−153.

(81) Theoretical surface coverages for ECMPS and CMPS SAMs were estimated using Scheme 1 and the following two equations: (A) coverage (CMP molecules·cm^{-2}) ≅ (10^{16} Å^2·cm^{-2})/X, where X = footprint area (Å^2/molecule) from Scheme 1; (B) coverage (mol of CMP·cm^{-2}) ≅ coverage (CMP molecules·cm^{-2})/6.023 × 10^{23} CMP molecules·mol of CMP^{-1}). The average spacing for the CMPS SAM tested as an imaging layer, assuming a square array of CMP groups on the surface: molecular spacing (square array) ≅ [(10^{16} Å^2·cm^{-2})/CMPS coverage (CMP molecules·cm^{-2})]$^{0.5}$ ≅ [(10^{16} Å^2·cm^{-2})/{(2.84 ± 0.22) × 10^{14}} CMPS molecules·cm^{-2}]$^{0.5}$ ≅ 5.9 ± 0.3 Å·CMP molecule^{-1} ≅ 0.6 nm·CMP molecule^{-1}.

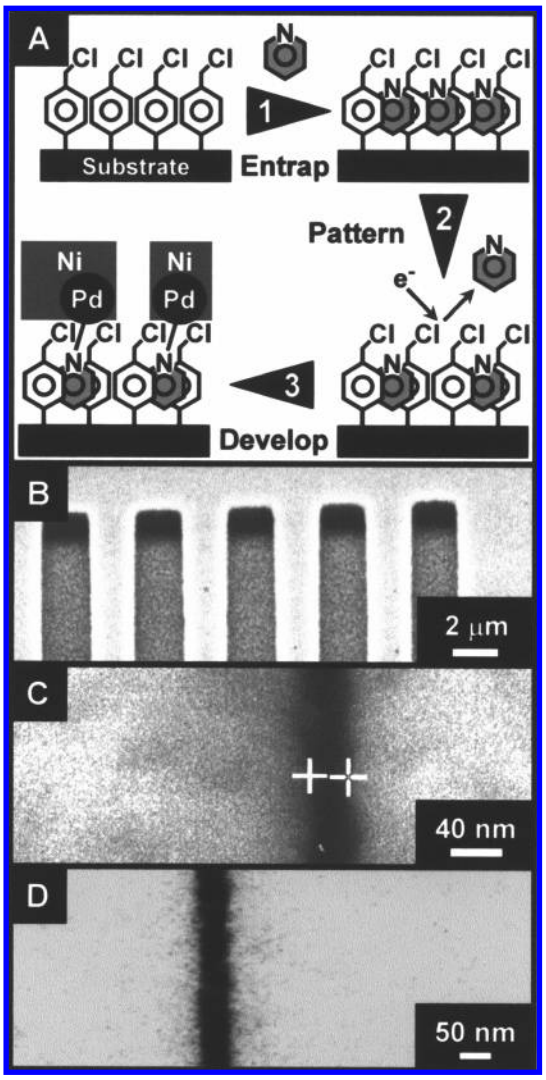

Figure 5. Evaluation of CMPS SAMs as lithographic imaging layers. (A) Scheme showing patterning and selective electroless metallization processes for the CMPS SAMs. The final RIE step following development of the latent image using the Pd catalyst and electroless Ni bath is not shown. Process sequence: (1) 0.1 M aq pyridine (3 h, 23 °C), (2) 500 $\mu C \cdot cm^{-2}$ (50 keV e-beam), (3) Pd (2 h, 23 °C),[27] (4) 10% NIPOSIT 468B Ni bath (6 min, 25 °C), and (5) RIE ~0.25 μm depth (16 sscm:12 sscm SF_6:CHF_3, 45 W, 18 mTorr, ~35 min). Parts B−D show SEM images of etched Si features (dark areas) in Ni metal fields (light areas) prepared according to this process. (B) Line-space pairs (2 μm × 2 μm). (C) A single ~30 nm wide line. The distance between the crosshairs is 30.7 nm. (D) A single 50 nm wide line. All Ni films are ~20 nm thick.

multilayer film patches occupying a few square nanometers of surface area on CMPS SAMs can influence patterning doses, compromising latent image formation and pattern fidelity in those areas for nanoscale features.[26] Consequently, it is important to assess the uniformity and quality of the SAMs over macroscopic film areas.

Therefore, in order to assess their uniformity and performance as imaging layers, we fabricated micro- and nanoscale line features (line widths ~ 2 μm to 30 nm) in Ni metal on a 2 in. diameter Si wafer bearing our CMPS SAM, corresponding to surface C of Figure 1, according to the protocol described in Figure 5A. Our approach[27,29,32,53] exploits the toluene solvent-templated defects and lower CMP surface coverages inherent in our SAMs by utilizing the nanocavity defects formed as sites for entrapping a pyridine ligand in step 1. Strong noncovalent binding of the pyridine inside the nanocavities, promoted by the formation of favorable van der Waals and/or $\pi-\pi$ interactions with the adjacent CMP groups and the geometric size match of the pyridine with the toluene-templated defect,[29,32] are sufficient to temporarily stabilize the bound pyridine under high vacuum conditions during e-beam patterning of the SAM in step 2. High-energy electrons successfully displace the adsorbed pyridine, creating the pattern latent image in the SAM.[27,29,32] Selective ligand binding of a Pd nanoparticle, which subsequently catalyzes electroless Ni deposition, at the remaining entrapped pyridine sites via step 3 develops the latent image as visible Ni features.[82]

Figure 5B shows one of several blocks of 2 μm line width Ni features prepared according to Figure 5A after reactive ion etching (RIE). Because electroless Ni films exhibit excellent etch resistance to the SF_6:CHF_3 etch plasma used,[27,29,32] they provide a convenient means to qualitatively assess SAM performance. Any failure of the patterning process in Figure 5A leading to Ni deposition on the e-beam-exposed SAM regions will be readily detected as Si protuberances[34] due to Ni particle etch masking during the RIE. We observe no such features in Figure 5B; the channel floors and sidewalls of the etched regions are smooth and clean. In addition, the patterned Ni features themselves clearly exhibit sharp, well-defined line edges and uniform width along the length of each line. These behaviors are consistent with good uniformity of the CMPS SAM and reproducibility of the process of Figure 5A, at least for the fabrication of microscale features.

Similar behavior is observed for nanoscale patterns, such as the ~30 nm wide line in the Ni film shown in Figure 5C. In this case, however, line width variations of at least 10% are observed in the Ni plated sample. For even smaller features, edge acuity and line width variations are increasingly more difficult to control. For example, we have previously observed line width variations exceeding 20% in ~15 nm wide lines fabricated in a Ni plated aromatic PEDA SAM patterned using low-energy electrons from an STM tip.[67] In both cases, these variations clearly exceed the 5% design rule required for electronic circuit fabrication, which has been satisfied only for ~50 nm width and larger features in Ni using our CMPS SAM (note Figure 5D).[27,29]

The inability to adequately control line edge acuity and pattern fidelity noted here for sub-30-nm features originates with the Ni plating methodology used to "develop" the SAM latent image created during the patterning step in Figure 5A. Because the growth of electroless Ni from each Pd catalyst particle under our processing conditions is isotropic, lateral growth of the Ni deposit over the latent image with increased plating time will eventually compromise pattern fidelity, especially as Ni particle size becomes an appreciable fraction (e.g., >20%) of the feature dimension. Ni particle sizes in our system are primarily determined by two factors: (1) Pd catalyst particle size and polydispersity and (2) surface ligand density, which is proportional to CMPS SAM coverage in this case. In particular, Ni particle size correlates directly with the size of the Pd catalyst, with larger catalyst particles producing larger Ni particles during the electroless deposition process.[65] Consequently, Ni edge acuity will be governed by the largest Pd particles present in the catalyst dispersion used to develop the latent image. Although the Pd catalyst dispersion[27] used to Ni plate the features shown in Figure 5 comprises particles having small average diameter (~2.6 ± 0.8 nm) and is nearly monodisperse (particle diameter range

(82) Attempts to utilize ECMPS films as imaging layers were not made. Preliminary experiments suggest that pyridine ligand is more readily desorbed from ECMPS films than CMPS films under the high vacuum conditions required for e-beam patterning. This behavior is consistent with (1) somewhat larger ECMPS nanocavity sizes due to decreased ECMPS surface coverage compared to CMPS (Scheme 1) and (2) destabilization of the ECMPS nanocavity by the flexible ethyl group, leading to hindered metallization.

∼1.5−5.0 nm; see Supporting Information Figure S-1), approximately 8% of its constituent particles have diameters of ∼4−5 nm (i.e., ∼13−17% of the 30 nm feature size).

Surface ligand density also influences Ni line edge acuity and pattern fidelity by regulating the binding of Pd nanoparticles comprising the catalyst distribution to the surface. For example, we have shown elsewhere[65,83] that surfaces having low densities of ligand sites preferentially bind the smaller, higher surface energy, Pd nanoparticles present in our catalyst dispersions. This provides a distinct advantage for the use of our CMPS SAMs, whose lower surface coverage leads to correspondingly sparse pyridine ligand surface densities in the fabrication of SAM latent images and their development via electroless metallization. This advantage is reinforced by further diminution of the ligand surface density resulting from inadvertent SAM exposure at the latent image edges due to scattered or stray incident 50 keV electrons and secondary electrons generated within the substrate during patterning.[27,29,32] These effects mitigate, at least partially, those attributed to the polydispersity of the Pd nanoparticles in the catalyst dispersion, permitting the fabrication of sub-30-nm features in Ni metal, albeit with noticeable loss of edge acuity and pattern fidelity.

The fabrication of even smaller features exhibiting acceptable edge acuity and line width control for the characterization and exploitation of our CMPS SAMs as efficient nanoscale imaging layers will clearly be dictated by our abilities to better control each of the patterning, catalysis, and metallization processes. Among these, the "development" steps associated with catalysis and Ni plating represent the greatest obstacles in properly assessing the imaging performance of our CMPS SAM. For example, the ultimate resolution achievable for our CMPS SAMs corresponds approximately to the ∼0.6 nm average spacing between adjacent CMP groups.[81] The smallest aromatic siloxane SAM latent images of ∼8 nm width currently available, fabricated in a PEDA SAM using an STM tip, are approximately an order of magnitude larger than this molecular limit. However, they are still substantially smaller than the best available ∼50 nm features in Ni films[29] (note Figure 5D) satisfying the 5% line width variation and edge acuity requirements for maintenance of pattern fidelity during development of the latent image. Addressing these challenges will undoubtedly require (1) the development of sub-2-nm-diameter noble metal nanoparticles of controlled shape, size, and polydispersity[84−86] as new electroless catalysts; (2) the use of electroless baths that ideally plate amorphous,[87−89] rather than crystalline, metal deposits; and (3) the reformulation of electroless baths to encourage anisotropic,[90,91] rather than isotropic, metal deposition to better control lateral metal growth during metallization. We are currently pursuing such options[92−94] to improve our nanolithography processing techniques and enable more accurate assessments of the quality and resolution limits of the CMPS SAMs described here.

Acknowledgment. We thank the Office of Naval Research (ONR) and the Naval Research Laboratory (NRL) for financial support for this work under the NRL Core 6.1 Program.

Supporting Information Available: Transmission electron micrograph of the Pd catalyst particles with a histogram showing the Pd particle size distribution. This material is available free of charge via the Internet at http://pubs.acs.org.

LA703326M

(83) Price, R. R.; Dressick, W. J.; Singh, A. *J. Am. Chem. Soc.* **2003**, *125*, 11259−11263.

(84) Park, J.; Joo, J.; Kwon, S. G.; Jang, Y.; Hyeon, T. *Angew. Chem., Int. Ed.* **2007**, *46*, 4630−4660.

(85) Burda, C.; Chen, X.; Narayanan, R.; El-Sayed, M. A. *Chem. Rev.* **2005**, *105*, 1025−1102.

(86) El-Sayed, M. A. *Acc. Chem. Res.* **2001**, *34*, 257−264.

(87) Georgieva, J.; Armyanov, S. *J. Solid State Electrochem.* **2007**, *11*, 869−876.

(88) Osaka, T.; Okinaka, Y.; Sasano, J.; Kato, M. *Sci. Technol. Adv. Mater.* **2006**, *7*, 425−437.

(89) Cui, M. Q.; Zhang, Z.; Zhang, M. J.; Huang, C. J. *Rare Met. Mater. Eng.* **2006**, *35*, 241−244.

(90) Lin, K-L.; Wu, C-H. *J. Electrochem. Soc.* **2003**, *150*, C273−C276.

(91) Vanderputten, A. M. T.; Debakker, J. W. G. *J. Electrochem. Soc.* **1993**, *140*, 2229−2235.

(92) Kostelansky, C. N.; Pietron, J. J.; Chen, M-S.; Dressick, W. J.; Swider-Lyons, K. E.; Ramaker, D. E.; Stroud, R. M.; Klug, C. A.; Zelakiewicz, B. W.; Schull, T. L. *J. Phys. Chem. B* **2006**, *110*, 21487−21496.

(93) Dinderman, M. A.; Dressick, W. J.; Kostelansky, C. N.; Price, R. R.; Qadri, S. B.; Schoen, P. E. *Chem. Mater.* **2006**, *18*, 4361−4368.

(94) Dobisz, E. A.; Brandow, S. L.; Chen, M-S.; Dressick, W. J. *Appl. Phys. Lett.* **2003**, *82*, 478−480.